Iranian Journal of Medical Physics

ijmp.mums.ac.ir

Development of a Liver Phantom Based on Computed Tomography Images for Dosimetric Purpose

Seyed Alireza Mousavi Shirazi

1. Department of Physics, South Tehran Branch, Islamic Azad University, Tehran, Iran.

ARTICLE INFO

Article type:
Original Article

Article history:
Received: Oct 15, 2017
Accepted: Jan 08, 2018

Keywords:
Computed Tomography
Dosimetry
Imaging
Liver
Phantom

ABSTRACT

Introduction: The present study was conducted with the aim of designing a liver phantom for dosimetry. To benchmark the results obtained by the developed liver phantom, another method was applied for the dosimetry of a real liver tissue using imaging.

Materials and Methods: For the purpose of the study, a real liver tissue was converted into a phantom based on the gram-molecular weight of the components of human liver tissue, mass percentage, and density, and then simulated by MCNPX code for dosimetry. The real liver tissue was contoured using the computed tomography DICOM images of the abdomen region. Subsequently, the accurate geometry of the segmented liver tissue was generated and simulated by MATLAB software and MCNPX code for dosimetric purposes. Then, the obtained data were transferred into the MCNPX code.

Results: Equivalent dose was measured in total and for each component of the liver phantom and separated liver tissue. The results obtained from these two simulations were compared with each other to validate the efficiency of the phantom and evaluated the differences.

Conclusion: The comparison of the equivalent doses obtained from the prepared equivalent liver phantom and the real liver tissue revealed the applicability of the liver phantom as a virtual liver for dosimetry.

► *Please cite this article as:*
Mousavi Shirazi SA. Development of a Liver Phantom Based on Computed Tomography Images for Dosimetric Purpose. Iran J Med Phys 2018; 15: 183-191. 10.22038/ijmp.2018.27035.1277.

Introduction

The liver tissue is one of the most sensitive organs of human body. Nowadays, the liver cancer is one of the most common cancers all over the world [1]. During radiotherapy, it is always essential to limit the dose to the normal tissues. On the other hand, the measurement and evaluation of absorbed dose is an issue of fundamental importance. Regarding this, a phantom modeling might be very useful for dose calculation before the implementation of the treatment. MCNPX code is an appropriate software tool facilitating this aim [2].

Some phantoms, such as MIRD, test phantom, and water phantom, are applicable for dosimetry. The MIRD and the Stylized Family phantoms were the first anthropomorphic phantoms; however, they represented the internal organs with simple mathematical equations [3]. The test phantoms are mainly comprised of cubes and isocenter circles applied for testing the accuracy of dose calculation. Currently, water phantoms are employed for clinical dosimetry. This phantom contains a water chamber, and a counter is placed at its various points [4, 5 6].

The existing liver phantoms used for dosimetric purposes have limitations. For instance, one of the models is a small-scale dosimetry model for various source-target combinations inside the micro-architecture of human liver [6 5]. Another model is the simulation of the liver lobule consisting of a single usual hepatic lobule. These phantoms usually measure absorbed dose with a noticeable degree of uncertainty.

Cancer therapy by X-ray photons is one of the most common therapeutic courses in medical radiation.

The present study was conducted with the aim of designing a new liver phantom as a substitute for real human liver that can be applicable for dosimetry in order to investigate the beam behavior in the liver tissue. To verify the efficiency of the developed liver phantom, a quite different dosimetric method was applied for a real liver tissue using the DICOM images of computed tomography (CT) scan. Subsequently, the dosimetry results obtained from the designed phantom and the real liver tissue were compared.

Materials and Methods

Design and simulation of phantom by MCNPX code

In this study, a spherical model of liver phantom was defined and simulated by MCNPX code. This phantom can have variable radii; in other words, it can be bigger or smaller than the dimensions applied in

*Corresponding Author: Department of Physics, South Tehran Branch, Islamic Azad University, Tehran, Iran. Tel: +98-9122027059; Fax: +98-2133060909; Email: a_moosavi@azad.ac.ir; alireza_moosavi@yahoo.com

this investigation. It is very difficult to determine the geometry and precise volume of the real liver tissue due to its non-uniform shape. Since the main aim of the research was to turn the real liver tissue into a hypothetical model, a spherical model was considered due to its symmetry. This model consisted of materials analogous to the components of a human liver tissue (weighing 2 kg), and each layer of the model met the related dimension.

This model of phantom had compositions and components similar to those of a human liver tissue (Table 1). After analyzing the structural components of the liver tissue based on their mass percentage and density into their constituent elements, consisting of hydrogen, oxygen, carbon, sulfur, and nitrogen, the amounts of these elements were calculated as accurately as possible. The calculation procedure of material amounts and determination of the prepared model dimensions were carried out based on the calculation of the gram-molecular weight of the existing materials in the human liver tissue.

The liver tissue is the second largest single organ in the body (after skin), weighing 2 kg (more than 1.44 kg) in an average and healthy adult [7 9]. The normal width, height, and depth of the human liver tissue are almost 21-22.5, 15-17.5, and 10-12.5 cm, respectively [8 10]. The advantage of the proposed spherical model is that this model is simple and flexible, consisting of all constituent materials in a real liver tissue. Moreover, the beam path has accurately been considered in this phantom. The laboratory experiments provided the precise molecular components of the liver tissue. The equivalent materials of the simulated liver are tabulated in Table 1.

Table 1. Molecular composition and structural materials of a real liver tissue [7 9]

Material	Mass percentage
Water	69.69%
Glycogen ($C_{24}H_{42}O_{21}$)	0.35%
Protein and Glucose ($C_{44189}H_{71252}N_{12428}O_{14007}S_{321}$ and $C_6H_{12}O_6$)	29.9%

Each of the existing components in the liver tissue was decomposed into its constituent elements. This decomposition was carried out based on the gram-molecular weight of existing components in the human liver tissue, mass percentage, and density of each element. Then, the accurate mass of every decomposed element (i.e., H, O, C, N, and S), existing in the constituent materials of the liver tissue, was accorded with the mass of the phantom components.

After decomposing the structural components of the liver tissue, the amounts of H and O were incorporated into the water. Furthermore, the amounts of other elements, namely C, S, and N, were calculated as accurately as possible. The phantom was configured by using a water sphere at the center, followed by an inner layer of carbon and a thin layer of sulfur, respectively. The whole body of phantom was encased in an outer carbon layer as a spherical shell. The large space, locating between this shell and the sulfur layer, was completely filled up with nitrogen gas.

The main reasons of the consideration of the mentioned arrangement in the phantom were as follows:

- Water was located at the middle of the phantom due to its physical state (fluidity) and because of considering water sphere as an integrated shape and not a layer.
- High-energy photons can cause the water molecule to be broken off, resulting in the release of the hydrogen atom (H^+ ion) into other parts.
- Since one of the elements extracted from the decomposition of the liver tissue was carbon, its amount was taken apart into both inner and outer layers. The main part of carbon was included in the inner layer around the water sphere (thicker part), and the thinner part was attributed to the outer layer (i.e., shell) of the phantom because of having the role of a case for the phantom.
- Regarding the low amount of sulfur as the componential element of the liver tissue, the inner carbon layer was surrounded by a very thin sulfur layer.
- Nitrogen composed the major part of the decomposed elements of the liver tissue. Given its gas state, the photons emitted from the source are able to cross this element to reach the first inner layer of the phantom.

Although the decomposition into various components may result in loosing the mixture homogenization, the phantom model was intended a new approach to be adopted designed for dosimetry in all components of the phantom and the liver tissue. The phantom was designed using the materials analogous to the components of a real liver tissue. In addition, each layer was accorded with the given dimension and filled up with the related material.

The phantom was comprised of a water sphere with a considered radius of 2.73 cm. The water sphere was covered with a layer of carbon (Table 2) with the hypothetical outer radius and thickness of 3.43 cm and 7 mm, respectively. There was an outer thin layer of sulfur with the thickness of 200 μm, covering the surface of the carbon layer. This set was wholly encased in a spherical shell of carbon as a reflector with the inner radius and thickness of 27.00 cm and 3.3 mm, respectively.

The blank space between sulfur layer and carbon shell was filled up with nitrogen gas. The space had the inner and outer radii of 3.45 and 27.00 cm, respectively.

The equivalent dose obtained for each of the portions could be generalized across the phantom. Water composes the main part of the liver tissue (i.e.,

almost 70%), and it is not considered as an inhomogeneous material [9 11].

The mass of each element, as well as the thicknesses and radii of hypothetical spheres are illustrated in Table 2.

Table 2. Mass, outside radius, and thickness of the analyzed elements

Elements	Mass (gram)	Outer radius of related sphere (cm)	Thickness (cm)
C	316.93	3.43 (inner carbon shell)	0.7
		27.33 (outer carbon shell)	0.33
S	6.08	3.45	0.02
N	102.94	27.00	23.55
H	198.90	Incorporated into the water sphere with a radius of 2.73 cm	
O	1373.93		

The phantom was comprised of a water sphere with a considered radius of 2.73 cm. The water sphere was covered with a layer of carbon (Table 2) with the hypothetical outer radius and thickness of 3.43 cm and 7 mm, respectively. There was an outer thin layer of sulfur with the thickness of 200 μm, covering the surface of the carbon layer. This set was wholly encased in a spherical shell of carbon as a reflector with the inner radius and thickness of 27.00 cm and 3.3 mm, respectively.

The blank space between sulfur layer and carbon shell was filled up with nitrogen gas. The space had the inner and outer radii of 3.45 and 27.00 cm, respectively. To better design this phantom, a hypothetical narrow beam path was also precisely considered as a cylindrical tube within the adipose tissue located in front of the liver tissue through which photons passed to reach the liver tissue.

In this study, the simulation was not limited to the inner parts of the liver phantom, because after the outermost layer (i.e., the shell around the phantom) where the photon beam path is, the width of this path is considered as the distance between clinical source and liver tissue, and the materials of it are considered as input data into the MCNPX code too. In other words, the X-ray photon passes across this cylindrical tube.

The path had a cylindrical form to play the role of a collimator. One of the most important tissues, laying in front of the liver, is adipose tissue. The adipose tissue is comprised of water, fat, and protein [10 12]. Water and fat normally constitute more than 90% of the body adipose tissue mass [11 13]. The adipose tissues have variant thicknesses (e.g., 0-10, 11-20, 21-30, and 31-40 mm) in different people, depending on their age and body mass index. In this investigation, the thickness of a normal adult adipose tissue (30 mm) was considered for the simulation [12 14]. One of the compositions of the adipose tissue is fat, which is a mixture of many esterified acids referred as fatty acids.

Regarding the skin tissue, the average skin thickness is lower in females, compared to that in males. The pure skin thickness is averagely 1.5 mm among males. The skin tissue and subcutaneous tissue consist of several parts, such as epidermis, dermis, hypodermis, and fat. Skin is a biological tissue composed of carbon, oxygen, nitrogen, a variety of proteins, water, fat, and salt [13 15]. The distance between body surface and liver tissue is around 3 cm in a normal body.

After the decomposition of both adipose and skin components into their constituent elements, given the mass and volume of each component, the inner and outer radii of the beam path were calculated with the highest possible accuracy. The mass values of each component in this cylindrical path and the path radii are shown in Table 3.

Table 3. Mass amount of each component and beam path radii

Compositions	Mass (gm)	Radii (cm)
Water	1.95	Incorporated into a cylindrical path with inside and outside radii of 1.5 cm and 2.1 cm, respectively
Fat	16.72	
Protein	0.40	

The side-view of the liver laying in the abdominal tissue and cylindrical beam path is displayed in Figure 1a. In addition, the schematic view of the liver phantom is illustrated in Figure 1b.

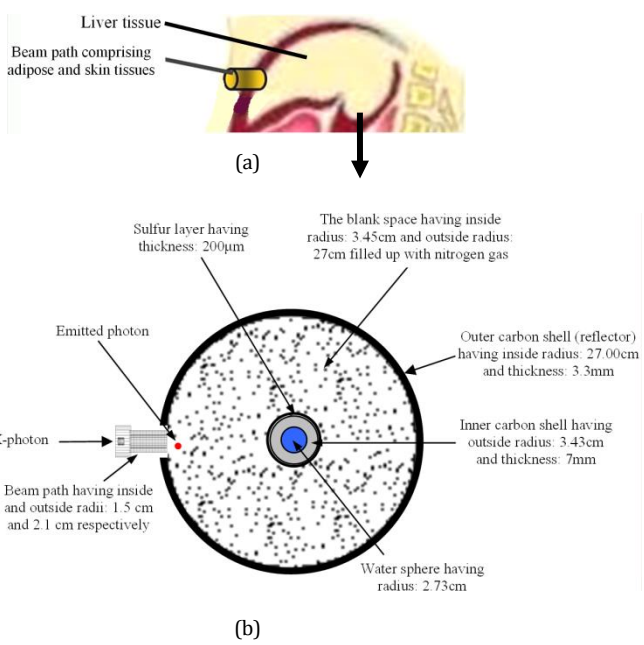

Figure 1. (a) Side-view of the cylindrical tube path and liver tissue (b) Schematic view of the liver tissue equivalent phantom

Figure 1a is the sketch of a real liver tissue, along with the mentioned X-ray photon beam path. The deposited energy in the phantom materials was computed by the MCNPX code. Figure 2 depicts the phantom simulated by MCNPX code.

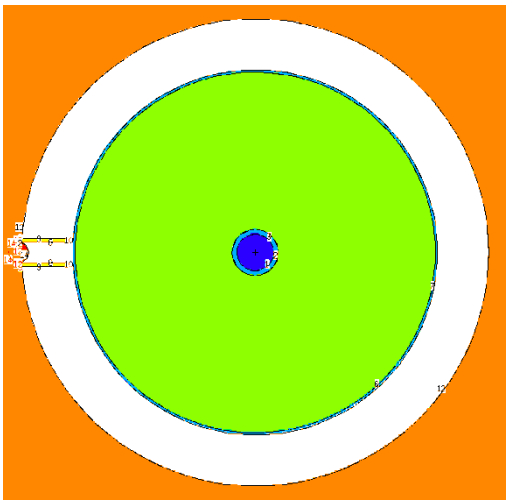

Figure 2. Liver equivalent phantom simulated by MCNPX code

For the purpose of simulation, the material-related and geometric data were entered into the MCNPX code; furthermore, the beam path was accurately taken into account.

Simulation and dosimetry of a real liver tissue by DICOM images, MATLAB software, and MCNPX code

The CT scan images of a male abdominal tissue (aged 45 years) were obtained using 80 keV photons applied from one direction at the Cartesian coordinates. In this study, the images were considered from XZ direction, in which the ventral view of the liver appeared. In the next stage, the scanned images were converted by MATLAB programming, which made a large number of volumes as voxels to build up full geometry of the tissue.

Each voxel was completely homogeneous and filled up with the related material (existing materials in the abdominal tissue) that had specific radiodensity, and each radiodensity was accurately correlated with that of the voxel.

After voxelization, the radiodensities of the organs in the abdominal tissue, having a large number of voxels, were defined, and the HU values were assigned to the generated voxels (Figure 3). Every part such as fat, bone, air, and water had its own radiodensity, defined based on the HU of each voxel. The HU values of other tissues were defined at the MATLAB software, and they were added to the previously defined materials.

All tissues located in the abdominal region were defined by these voxels. Each voxel had a specific CT number; therefore, each radiodensity was accurately correlated with CT number of the voxel. The Hounsfield unit (HU) values of some other body tissues were defined at the MATLAB software, and they were added to the previously defined materials.

Determination of the type of materials filling up the voxels

Type of each tissue was recognized by the mentioned program based on the level of grayness and CT number of all pixels in DICOM images. The existing voxels in the liver area were quite homogeneous and filled up with the constituent materials of the liver tissue [14 16]. All of the existing organs in the abdominal region were defined for the program according to the CT number or HU value using the following equation [15 17]:

$$\mathrm{HU} = \frac{\mu_X - \mu_{\mathrm{water}}}{\mu_{\mathrm{water}} - \mu_{\mathrm{air}}} \times 1000 \qquad (1)$$

where, μ_X is linear attenuation coefficient for material X, μ_{water} is linear attenuation coefficient of water, and μ_{air} is linear attenuation coefficient of air.

Tables 4 and 5 demonstrate the values of HU and linear attenuation coefficient for some of the tissues, respectively.

Table 4. Hounsfield unit values for some tissues and materials [16 18]

Tissue (material)	Hounsfield unit
Air	-1000
Fat	-100
Water	0
Muscle	+40
Blood	+40
Bone	≈>400 (>1200)
Aluminum	2640 (at 60keV)

Table 5. Linear attenuation coefficient values (in cm-1) for some tissues at different energies of X-ray photon [16 18]

Tissue (material)	40 keV	60 keV	80 keV	100 keV
Fat	0.228	0.188	0.171	0.160
Water	0.268	0.206	0.184	0.171
Bone	1.28	0.604	0.428	0.356
Aluminum	1.535	0.750	0.545	0.460
Titanium	10.05	3.48	1.840	1.235

The HU values for some of the tissues are tabulated in Table 6.

Table 6. Hounsfield unit values (at 80 keV) for various body tissues calculated for MATLAB programming [16 18]

Tissue	Hounsfield unit
Lung	-880
Breast	-150
Liquid	-2
Soft	1
Muscle	100
Bone	1851850

Contouring and separation of the voxelized liver tissue

In the programming, there were a large number of volumes as lattice to build up the geometry of the

tissue. There was a big lattice specified so that it could be divided into very small lattices. The resolution of small lattices might be arbitrary. In this study, the resolution of each small lattice was considered as 1 mm^3 since the minimum resolution of clinical X-ray imaging machine applied in this project was 1 mm^3. After voxelization and filling up the abdominal tissue with the given materials, the liver tissue was contoured and separated from other tissues located in the abdominal region. This contouring was carried out by filling up the rest of the existing materials in other parts with air.

Transferring data into MCNPX code and dose calculation

The accurate geometry of the separated liver tissue was generated by the MATLAB software as input data, and then transferred into the MCNPX code.

Then, the materials existing in the liver tissue (rather than those in other soft tissues) were defined as input data for MCNPX. Subsequently, the MCNPX program was run, and the accurate equivalent doses were obtained. The color of the reconstructed images was automatically determined by MCNPX code based on the material number at the organs of abdominal tissue.

Results

Some plots of abdominal region, converted by MATLAB software and MCNPX code, were consecutively illustrated in four stages as shown in Figure 4.

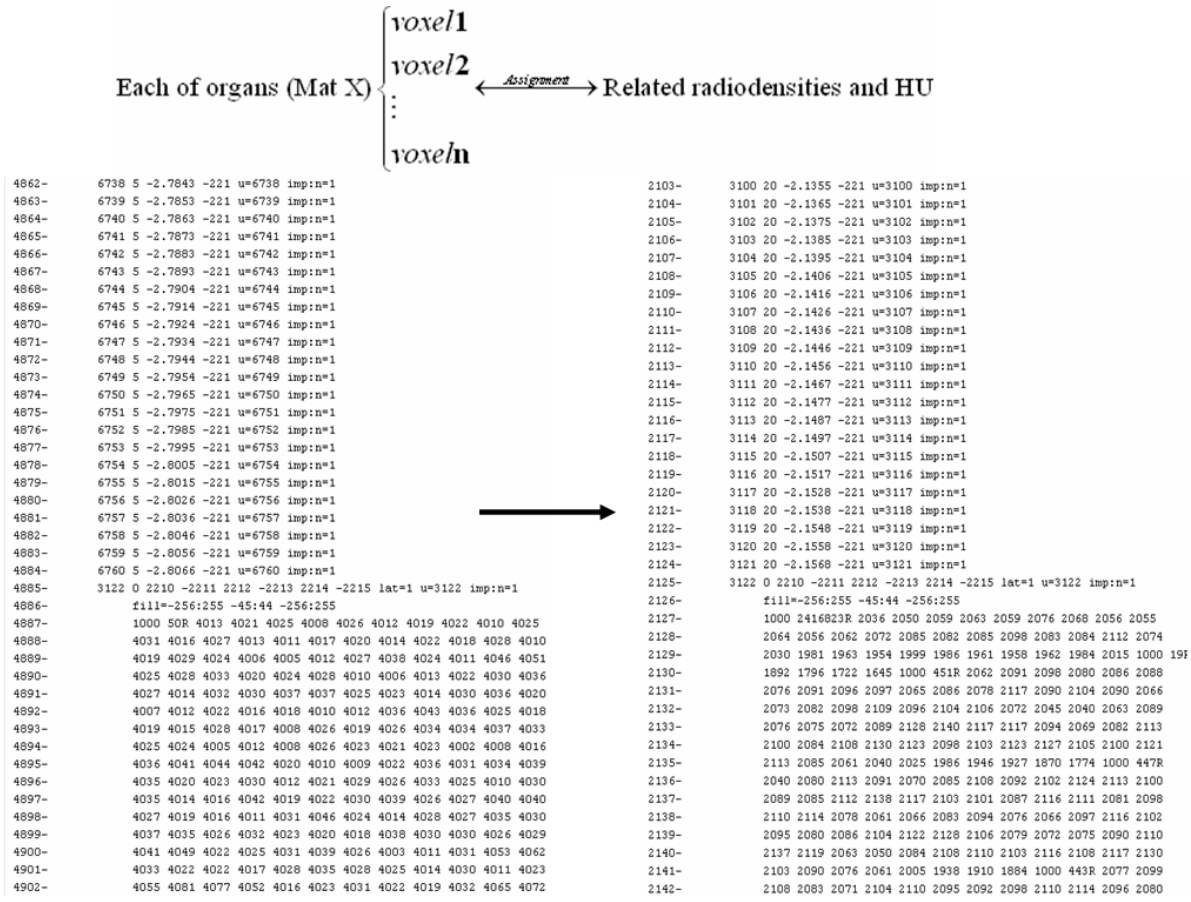

Figure 3. Generation of data by MATLAB program and their transference to MCNPX code

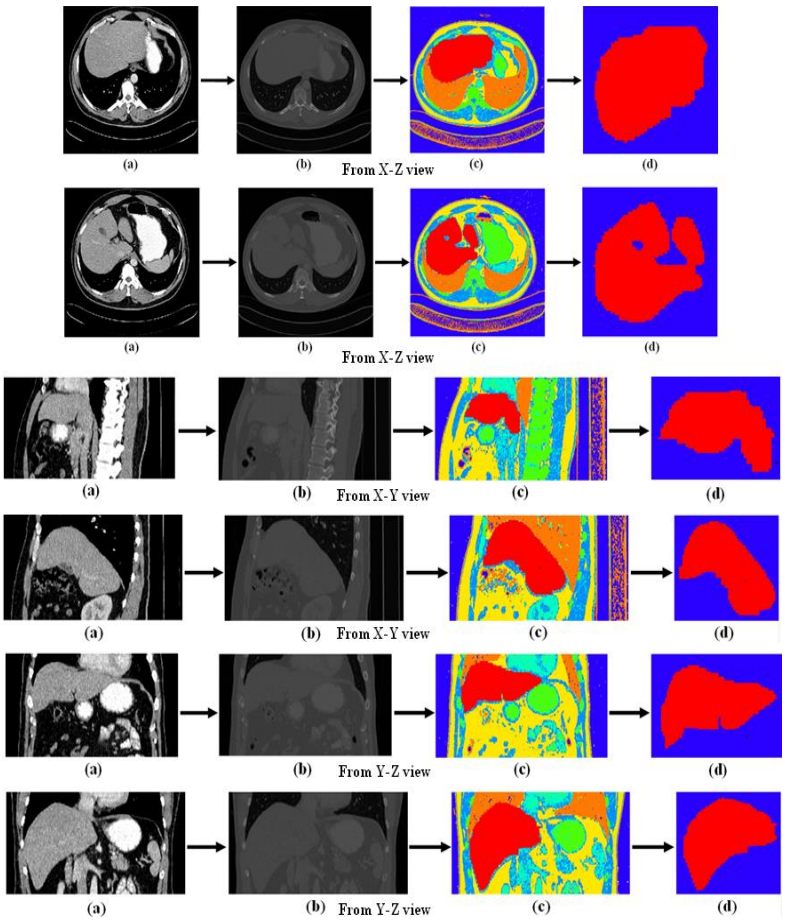

Figure 4. (a) Image of abdominal tissue slice using computed tomography scanning, (b) Image of abdominal tissue converted by MATLAB from computed tomography image, (c) Image of abdominal tissue converted by MCNPX from MATLAB , (d) Image of separated segmented liver tissue shown by MCNPX

Figure 5. Views of the liver phantom, real liver tissue, and separated segmented liver tissue

As observed in figures 4c and 4d, the liver tissue was determined in red. Figure 5 illustrates the equivalence among the real liver tissue, liver phantom, and separated segmented liver tissue (produced by both MATLAB and MCNPX code), resulting from the two simulations performed in this study.

To validate the efficiency of the phantom, equivalent doses were measured in total and for each component of the liver phantom and separated segmented liver tissue and compared with each other, considering the weighting factor of 1 for X-ray photons.

Figures 6-7 show the total amounts of equivalent doses in the liver phantom and the separated segmented liver tissue and also the relative error between two models, respectively.

The amounts of equivalent doses in the constituent elements of the liver phantom and the separated segmented liver tissue are illustrated in Figure 8. In addition, the differences between the two models are evaluated and shown in figures 9-12.

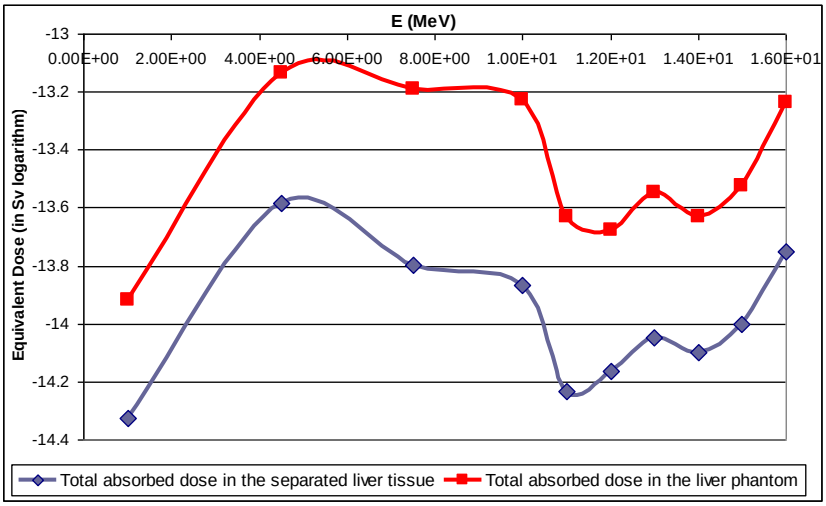

Figure 6. Total amounts of equivalent doses in both the separated real liver tissue and the liver phantom

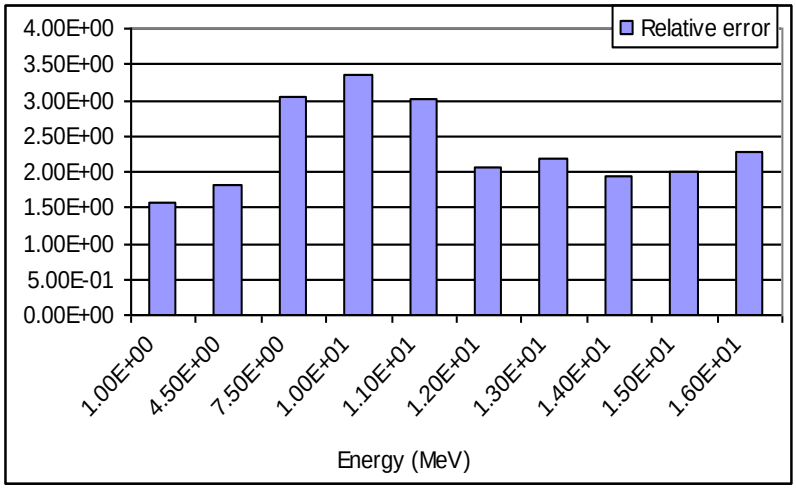

Figure 7. Relative error between two models for the total amounts of equivalent doses

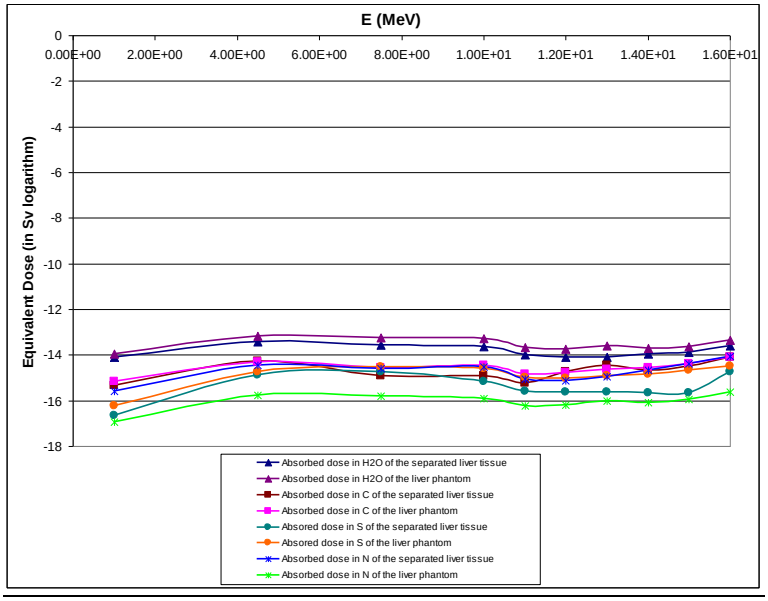

Figure 8. Equivalent doses in the components of liver phantom and separated segmented liver tissue

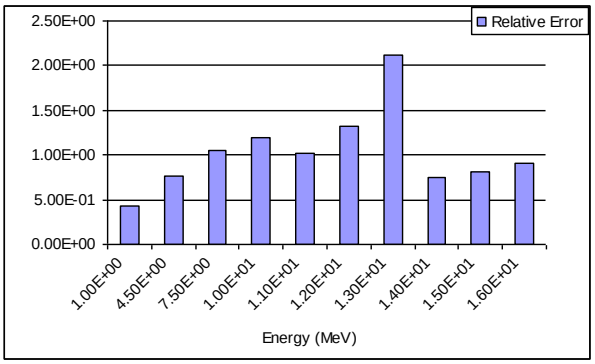

Figure 9. Relative error between two models for water

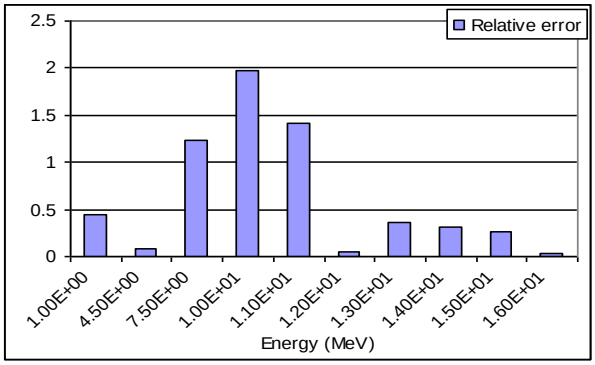

Figure 10. Relative error between two models for carbon

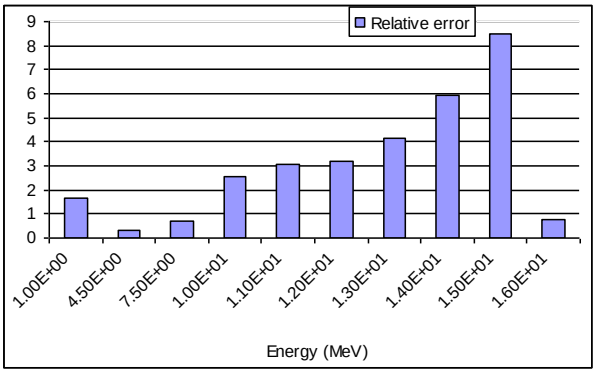

Figure 11. Relative error between two models for sulfur

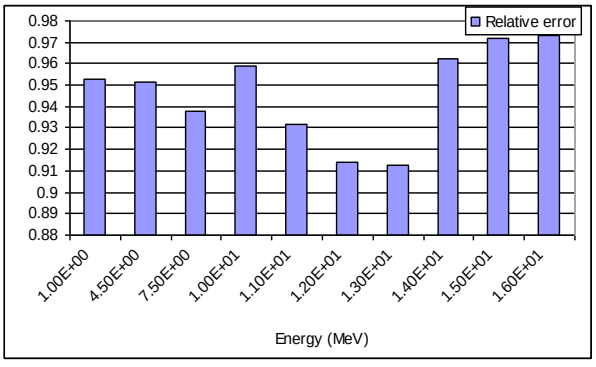

Figure 12. Relative error between two models for nitrogen

Discussion

In this study, a new liver phantom was designed using the equivalent tissue substitutes based on the gram-molecular weight, mass percentage, and density of the human liver tissue components. The designed phantom was simulated by MCNPX code and exposed by X-ray within the energy range of 1-16 MeV. Thereafter, the dosimetry of the existing materials was carried out in the phantom. In a different section of the research, the DICOM images of an abdominal tissue were considered.

With the aid of MATLAB software and DICOM images and using MCNPX code, the liver tissue surrounded by abdominal tissue was separated, and then irradiated by photon-X similar to the liver phantom. The dosimetry of the existing materials was also performed in the separated liver tissue. Finally, the obtained equivalent doses of the liver phantom and liver tissue components were compared with each other. The results revealed that this liver phantom can be applicable for dosimetry and investigating the behavior of photons on human liver tissue.

Based on Figure 6, within the energy range of 1-16 MeV (although the course of therapy by high-energy X-ray photons is outdated), the calculated total equivalent dose in the liver phantom was roughly similar to that of the real liver tissue, and their derived graphs were almost analogous. As indicated in figures 6 and 8, the maximum value of equivalent dose is escalated in almost 5 MeV. According to Figure 8, it can be concluded that water received the major amount of equivalent doses, and carbon, nitrogen, and sulfur received lower amounts, respectively.

It was also concluded that in proportion to the value of photon energy, the difference between equivalent doses for nitrogen was bigger than that for all other elements. On of the limitations of this study was the lack of reference values for some tissues, such as gallbladder wall and major blood vessels. Furthermore, modeling of the thin tissues, like skin and oral mucosa, was not practically possible. Additionally, the generation of lattices and voxels for the thin tissues required a large computer memory space. Moreover, the generation of lattices with rectangular shape increased the possibility of covering a little portion of other tissues. Therefore, it was impossible to define a segmented tissue completely close to that tissue, even though minimizing the air regions was possible.

Conclusion

The comparison of the amounts of equivalent doses obtained from the prepared liver phantom and the real liver tissue revealed a good agreement in this regard. Therefore, it was concluded that this phantom could be applied for dosimetric purposes and studying beam behavior in the liver tissue

components. As mentioned previously, in this research, a new liver phantom was designed just based on the gram-molecular weight, mass percentage, and density of the existing compounds in the human liver tissue.

The dimension of the phantom is flexible; accordingly, it can be bigger or smaller than the applied dimensions in the current investigation. These variations might be carried out for bigger or smaller size of the liver tissue. This phantom might be really equivalent to the dimensions of the livers belonging to either adult or adolescent or infant. This flexibility facilitates the consideration of a cancerous tumor or lump within the liver tissue and the decomposition of its constituent elements. In this regard, if components of the given tumor are H, O, C, S, and N, they are added to the amount of the existing elements in the liver tissue; otherwise, they are defined as a new layer. Furthermore, if the weight of the liver tissue is greater than the mean value, the thickness and radius of each sphere will be variable.

Regarding the application of the DICOM images of CT scan by dosimetry, it should be taken into consideration that this method can be performed for every patient through his/her own CT scan images to determine the permissible absorbed and equivalent doses following all the mentioned procedures.

References

1. Chakraborty S, Das T, Sarma H, Venkatesh M, Banerjee S. Preparation and preliminary studies on 177Lu-labeled hydroxylapatite particles for possible use in the therapy of liver cancer. Nuclear Medicine and Biology. 2008;35: 589-97.
2. Reginatto M. What can we learn about the spectrum of high-energy stray neutron fields from Bonner sphere measurements?. Rad Measur. 2009;44:692-99.
3. Mousavi Shirazi SA, Sardari D. Design and simulation of a new model for treatment by NCT. Sci Technol Nucl Ins. 2012; 2012:1-7. Doi:10.1155/2012/213640.
4. Kramer R, Cassola VF, Khoury HJ , et al. FASH and MASH: female and male adult human phantoms based on polygon mesh surfaces: II. Dosimetric calculations. Physics in Medicine and Biology. 2010;55:163-89.
5. Wambaugh J, Shah I. A Model for Micro-Dosimetry in Virtual Liver Tissues. The 10th International Conference on Systems Biology Stanford. 2009 August 31-September 4; California (USA).
6. Stenvall A, Larsson E, Strand SE, Jönsson BA. A small-scale anatomical dosimetry model of the liver. Phys Med Biol. 2014; 59:3353-71. Doi: 10.1088/0031-9155/59/13/3353.
7. Postuma I, Bortolussi S, Protti N, Ballarini F, Bruschi P and et al. An improved neutron autoradiography set-up for 10B concentration measurements in biological samples. Reports of Practical Oncology and Radiotherapy. 2016;21:123-8.
8. Koivunoro H, Bleuel D, Nastasi U, Lou T, Reijonen J and et al. BNEUTRON THERAPY dose distribution in liver with epithermal D–D and D–T fusion-based neutron beams. Applied Radiation and Isotopes. 2004;61:853-9.
9. McBride J, Mason M, Scott E. The Storage of the Major Liver Components. Biol Chem. 1941;1:943-52.
10. Clark H. The Cure for All Diseases (FE). New Century Press, 1995.
11. Högberg J, Rizell M, Hultborn R, Svensson J, Henrikson O, Mölne J , et al. Increased absorbed liver dose in Selective Internal Radiation Therapy (SIRT) correlates with increased sphere-cluster frequency and absorbed dose inhomogeneity. European Journal of Nuclear Medicine and Molecular Imaging. 2015; 2(1):10. Doi: 10.1186/s40658-015-0113-4.
12. Lorette WT. The Chemical Composition of Adipose Tissue of Man and Mice. Exp Physiol.1962; 47:179-88.
13. Martin AD, Daniel MZ, Drinkwater DT, Clarys JP. Adipose tissue density, estimated adipose lipid fraction and whole body adiposity in male cadavers. Int J Obes Relat Metab Disord. 1994;18:79-83.
14. Otte JW, Merrick MA, Ingersoll CD, Cordova ML. Subcutaneous adipose tissue thickness alters cooling time during cryotherapy. Arch Phys Med Rehabil. 2002;83:1501-5.
15. Broder V. Observations on skin thickness and subcutaneous tissue in man. Z Morph Anthrop. 1960;50:386-95.
16. Smith JT, Hawkins RM, Guthrie JA and et al. Effect of slice thickness on liver lesion detection and characterisation by multidetector CT. J Med Imaging Radiat Oncol. 2010; 54:188-93. Doi: 10.1111/j.1754-9485.2010.02157.x.
17. Hounsfield GN. Computed medical imaging. J RADIOL. 1980;61(6-7):459-68.
18. Reeves TE, Mah P, McDavid WD. Deriving Hounsfield units using grey levels in cone beam CT: a clinical application. Dentomaxillofac Radiol. 2012;41:500-8. Doi: 10.1259/dmfr/31640433.